Theor Chem Acc (2013) 132:1301
DOI 10.1007/s00214-012-1301-0

REGULAR ARTICLE

Density functional and chemical model study of the competition between methyl and hydrogen scission of propane and β-scission of the propyl radical

Marc E. Segovia · Kenneth Irving · Oscar N. Ventura

Received: 20 June 2012 / Accepted: 7 November 2012 / Published online: 5 December 2012

Abstract In this work, we study the competence between the reactions of hydrogen and methyl scission during thermal cracking and combustion of propane, the emergence of the two isomers of the propyl radical, *n*-propyl and *i*-propyl, and their subsequent β-scission reaction to ethene and methyl radical. The purpose of the study was to analyze the accuracy of density functional (DFT) methods as applied on this relatively well-known subset of the reactions implied in the production of propylene oxide from propane and propene. Conventional (B3LYP, B3PW91) and state-of-the-art (PBE0, M06, BMK) DFT methods were employed, and their accuracy checked against experimental data and calculations performed using model chemistries (complete basis set CBS-4M, QB3, and APNO, and G4 methods) and ab initio methods (MP2, CCSD(T) with a large 6-311 ++G(3df,2pd) basis set). The results obtained at the BMK level for the thermodynamics of the reactions are closer to experimental data than those afforded by any other DFT method and very similar actually to CBS or CCSD(T) results, even if a medium size basis set is used. Activation energies determined using two- and three-parameter Arrhenius equations are also very good, but the preexponential factors are incorrect. Tunneling and internal rotation corrections must be applied to obtain semiquantitative results.

Keywords Propane cracking · Density functional methods · BMK · Thermochemistry · Kinetics · CCSD(T) calculations · Composite models

1 Introduction

Hydrocarbon cracking is the name of the process by which higher molecular weight hydrocarbons are converted into lower molecular weight species, through carbon–carbon bond scission [1]. This process is central to obtain gasoline by petroleum refining, and several methods have been developed to make it more efficient.

Thermal cracking is the simplest and oldest method. It relies on the use of high temperatures (∼450°–750°) and pressures (up to about 70 atm.) to produce the scission of C–C and C–H bonds, producing radicals that then react with other neutral or radical species. Olefins are produced during this thermal process, especially high yields of ethylene and smaller amounts of alpha olefins, like propene for instance. Normally, cracking processes involve many species and hundreds of reactions, a reason for which the experimental studies of cracking reaction kinetics are very difficult [2–4]. On the other side, optimizing the performance of these processes for different raw materials and process conditions requires detailed and accurate kinetic models and, thus, the knowledge of precise thermodynamic and kinetic data [5, 6].

Computational chemistry has advanced dramatically in the last decades, due to the increase in the availability of moderately priced hardware and software and may be an alternative or complementary method to study the thermodynamics and kinetics of cracking processes. It is well known that very accurate total and relative energies of molecular species can be obtained at the coupled cluster

Dedicated to Professor Marco Antonio Chaer Nascimento and published as part of the special collection of articles celebrating his 65th birthday.

M. E. Segovia · K. Irving · O. N. Ventura (✉)
Computational Chemistry and Biochemistry Group (CCBG), DETEMA, Facultad de Química, UdelaR, CC1157 Montevideo, Uruguay
e-mail: onv@fq.edu.uy

CCSD(T) level when a sufficiently large basis set is used. Regretfully, this method is computationally very demanding and can be applied routinely only to small molecules. Therefore, simpler methods, which may be applied to larger molecules, need to be gauged against accurate CCSD(T) calculations and experimental data, when available.

In this paper, we describe a computational study of the cracking reactions of propane and the production of olefins, especially propene, as a preliminary step in our research of gas-phase production of propylene oxide. The purpose of the study is twofold. On the one hand, we aim to compare different computational schemes applied to a subset of reactions for which experimental data exist. On the other hand, we want to obtain precise estimates of the thermochemistry and kinetics of the radical chain initiation, propagation and termination reactions involved in the mechanism. Previous computational and experimental studies on this area of research have been performed by several authors, which results we will use to compare to our own.

Sabbe et al. [7] did the most recent theoretical calculations in 2007. The composite methods CBS-QB3 and G3B3, as well as density functionals MPW1PW91, BB1 K, and BMK, were used with several corrections for tunneling and internal rotation for the calculation of rate coefficients for carbon-centered radical addition and β-scission reactions. They found that the DFT-based values for β-scission rate coefficients deviate significantly from the experimental ones at 300, and the DFT methods do not accurately predict the equilibrium coefficient. Zheng and Blowers[8] published in 2006 an investigation of the propyl radical β-scission reaction kinetics and energetics using quantum chemical Gaussian-3 (G3) method and a specially designed complete basis set (CBS) composite energy method. Good agreement with experimental results was reported for the CBS calculations. Curran [9] in 2006 determined rate constant expressions for C1-C4 alkyl and alkoxy radicals decomposition via β-scission based on the reverse, exothermic reaction, the addition of a hydrogen atom or an alkyl radical to an olefin or carbonyl species with the decomposition reaction calculated using microscopic reversibility on the basis of experimental data. Hunter and East [10] studied theoretically, at the B3LYP, MP2, CCSD(T), and G2 levels, the bond strengths of the C–C bonds in alkanes up to $C_{20}H_{42}$. Bond strength was found to be very constant (88 kcal mol^{-1}), except for the α and β bonds (89 and 87 kcal mol^{-1}, respectively). For thermal cracking, the results suggest that the most favored initiation step is the breaking of the β bond of the alkane to create an ethyl radical. Xiao et al. [11] in 1997 performed UHF and DFT calculations to investigate the detailed kinetics and mechanisms of hydrocarbon thermal cracking. They studied specifically the bond dissociation energy (BDE) for C–C homolytic scission—a process occurring without transition states—finding values of about 95 kcal/mol at the MP2/6-31G* level and 89 kcal/mol at the B3LYP/6-31G* level. H-transfer reactions do exhibit transition states, as expected, with activation energies of about 15–17 kcal/mol at the MP2/6-31G* level and 10–12 kcal/mol at the B3LYP level. Finally, they found an activation energy for β-scission of about 30–33 kcal/mol, while the activation energy for the reverse addition reaction was found to be about 5 kcal/mol. The optimized transition state structure is product-like for the radical decomposition reaction and reactant-like for the addition reaction.

Bencsura et al. [12] in 1992 produced the most recent experimental data on the reaction kinetics of the propyl radical, based on previous work. Radicals were produced by pulsed laser photolysis and their unimolecular decay subsequently studied by photoionization mass spectrometry. Tsang [13] in 1988 produced a compilation of revised and evaluated data on the kinetics of reactions involving propane and the propyl radical, among other species. The general mechanism for the decomposition of propane was initially determined by Papic and Laidler [14, 15] who experimentally identified most of the products which are consistently predicted in the mechanism proposed in this paper. We followed their rationale for the development of our own model.

2 Methods

Ab initio, density functional (DFT) and model chemistry methods have been used in this paper. B3LYP [16–18], B3PW91 [16, 17, 19], PBE0 [20–22], M06 [23] and BMK [24] DFT geometry optimizations [25] and analytic frequency [26–28] calculations were performed using the 6-31G(d,p) (basis I), 6-311 +G(d,p) (basis II), and 6-311 ++G(3df,2pd) (basis III) Pople basis sets, as representative of small, medium, and large polarized basis sets. Post-Hartree–Fock second-order Møller–Plesset (MP2 [29–32]) geometry optimizations and frequency calculations were performed using only the larger basis set. For a small set of molecules, CCSD(T) [33, 34] frequency calculations were performed on the MP2 optimum geometries, using also the larger basis set. Complete basis set (CBS) model chemistry methods [35–41], namely CBS-4M [39], CBS-QB3 [39, 40], and CBS-APNO [41], were also employed to calculate thermodynamic properties of all stable reactants, products, and intermediate radicals, but not for transition states. Those calculations were also performed using Curtiss Gaussian-4 theory (G4) [42].

The choice of DFT methods employed in the calculations was not arbitrary. The default choice is the

adiabatically corrected (or hybrid) B3LYP method, which gives fairly accurate results and has been widely used in the last decade. We ourselves prefer B3PW91—that is, with a different choice of the correlation energy potential—because we showed in a number of publications that both methods usually agree, but when they do not, then B3PW91 is closer to the experimental results than B3LYP. The reason is that the fitting parameters in B3LYP were actually not fitted but taken from B3PW91. The three other methods chosen represent the implementation of increasingly complex and accurate methodologies. PBE0 is the adiabatically coupled version of the non-empirical potential of Perdew, Burke, and Erzenhoff. M06 is a meta-hybrid GGA method which depends not only on the Laplacian of the density, but also on the spin kinetic energy density. The method depends on several parameters which are adjusted on a training set and is particularly suited to describe non-covalent interactions. Finally, the BMK DFT method includes also the spin kinetic energy density, but it is fitted to thermochemical and kinetic data, so that its main field of applicability is to study thermochemical and kinetic properties of chemical reactions.

Basis sets of different complexity were used with the DFT methods in order to assess their accuracy, since it is known that DFT methods do not depend so heavily on the basis set size as ab initio methods do. The most exact ab initio calculations performed in this paper are the CCSD(T)//MP2/6-311 ++G(3df,2pd) done on the smaller molecules. Regretfully, some of the species studied (depicted in the scheme in Fig. 1) were too large to follow this procedure. In those cases, the CBS-APNO results were considered as the nearer best and used for comparison to the presumably less accurate DFT and MP2 calculations.

Chemical models as CBS or Gn are also called composite energy methods or compound models and aim to reach high level of accuracy at a moderate cost through addition of energy corrections calculated at different levels. G4 is the latest in the series of Gn chemical models, an improvement over G3 theory. Geometries as well as zero point energies are determined using B3LYP DFT with the 6-31G(2df,p) basis set. Correlation level calculations are performed using Møller–Plesset perturbation theory up to fourth order and with coupled cluster theory. Large basis sets, including multiple sets of polarization functions, are used in the correlation calculations. The CBS methods, on the other side, rely on the extrapolation toward the complete basis set limit using the N^{-1} asymptotic behavior of N-configuration pair natural orbital (PNO) expansions. The more accurate method, CBS-APNO, includes up to QCISD(T)/6-311 ++G(2df,p) calculations for estimating the correlation energy.

Thermodynamic calculations were performed at 0 K, room temperature and 600 K, in all cases assuming atmospheric pressure. Rate constants were calculated using the standard canonical transition state theory with Eckart′s correction for tunneling [43] and both with and without hindered rotor treatment of the internal rotation. Rate coefficients are calculated based on conventional transition state theory in the high-pressure limit. For the bimolecular radical addition, the rate coefficient is calculated according to Eq. 1:

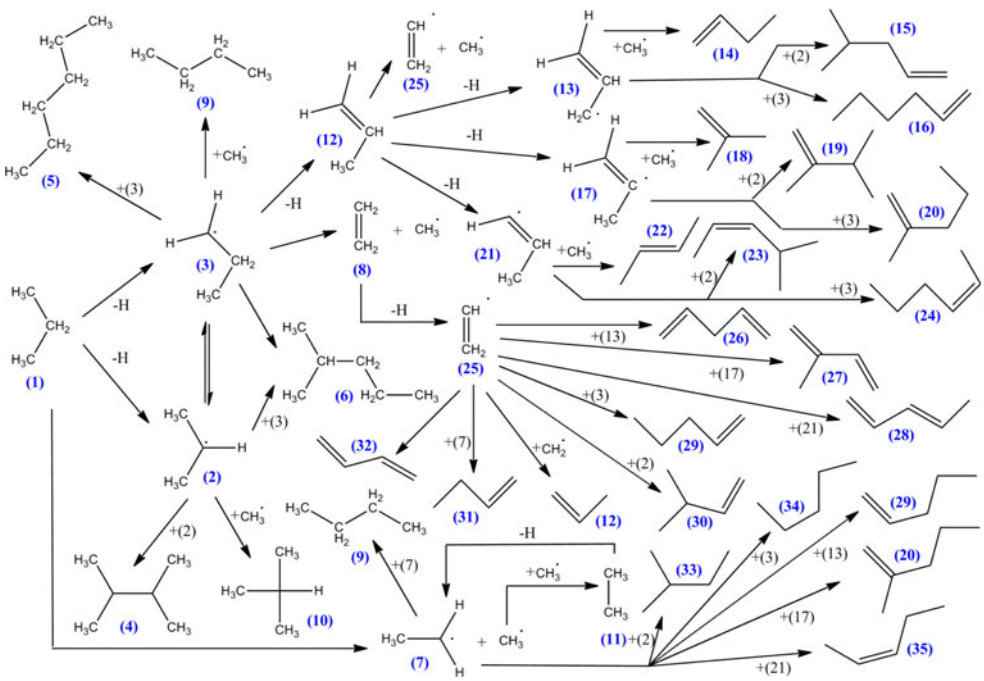

Fig. 1 Schematic depiction of the main reactants and products in the mechanism of cracking of propane

$$k\infty(T) = \kappa(T)(kBT/h) \left(n_{\mathrm{opt},\#}q^{\#}/n_{\mathrm{opt,A}}q^{\mathrm{A}}n_{\mathrm{opt,B}}q^{\mathrm{B}}\right)\mathrm{e}^{-\Delta\mathrm{E(0K)/RT}}.$$

The monomolecular rate coefficients are calculated according to:

$$k\infty(T) = \kappa(T)(kBT/h)\left(n_{\mathrm{opt},\#}q^{\#}/n_{\mathrm{opt,P}}q^{\mathrm{P}}\right)\mathrm{e}^{-\Delta\mathrm{E(0K)/RT}}$$

where q is the total molar partition function per unit volume, $\kappa(T)$ is the tunneling coefficient, and ΔE(0 K) is the activation barrier at 0 K including zero point vibrational energy (ZPVE). The number of optical isomers n_{opt} enters the equation because the partition functions are calculated for a single optical isomer whereas all configurations, including those that are not directly thermally accessible from the reference configuration, should be accounted for. External and internal symmetry numbers are contained within the partition functions.

Standard Arrhenius parameters A and E_a were derived from a regression of ln(k) against $1/T$ in the way

$$\ln k = \ln A - E_a/RT$$

Energies, geometries, frequencies, and other properties were calculated using the Gaussian 09 computer code [44]. The thermochemical and kinetic analysis were performed using the program TAMkin [45].

Figure 1 shows a general scheme of the species and reactions investigated in this paper. Forty-one chemical species were combined into 100 chemical reactions, to describe approximately the reaction system related to thermal cracking of propane in the absence of oxygen. Although possible from a theoretical point of view, we have not included in this study the CC and CH bond-breaking reactions of hydrocarbons larger than C_3H_8, generated by radical chain termination reactions. This decision was taken on the ground that the concentration of larger olefins is much smaller than those of propane, ethylene and related C_2 and C_3 species. Therefore, we expect that radicals generated from C_n species ($n > 3$) will be of marginal importance and were not included in the research.

3 Results and discussion

3.1 Initial steps

Modeling of thermal cracking of propane was performed by Sundaram and Froment [46] on the basis of experimental work by Van Damme et al. [47]. The kinetics of mercury-photosensitized decomposition of propane was studied in a pair of papers by Papic and Laidler [14, 15] in the seventies.

C–C and C–H bond breaking are possible decomposition reactions for propane, according to the following mechanisms

$$C_3H_8 \rightarrow C_2H_5\cdot + CH_3\cdot \quad (1)$$

$$C_3H_8 \rightarrow iC_3H_7\cdot + H\cdot \quad (2)$$

$$C_3H_8 \rightarrow nC_3H_7\cdot + H\cdot \quad (3)$$

$C_2H_5\cdot$ has only one structural conformer, while $C_3H_7\cdot$ is the global formula for two structural isomers, the 1-propyl ($nC_3H_7\cdot$) and 2-propyl ($iC_3H_7\cdot$) radicals, whose fates differ, as seen in Fig. 1. 2-propyl radical is more stable than 1-propyl radical at all levels, because of the stabilization produced by hyper-conjugation of the radical with the neighbor methyl groups. Both the hydrogen atom and the methyl radical produced in this chain initiation reactions can participate in dehydrogenation propagation reactions, in the form

$$C_3H_8 + H\cdot \rightarrow iC_3H_7\cdot + H_2 \quad (4)$$

$$C_3H_8 + H\cdot \rightarrow nC_3H_7\cdot + H_2 \quad (5)$$

$$C_3H_8 + CH_3\cdot \rightarrow iC_3H_7\cdot + CH_4 \quad (6)$$

$$C_3H_8 + CH_3\cdot \rightarrow nC_3H_7\cdot + CH_4 \quad (7)$$

We can use these first seven reactions to make a primary analysis of the performance of different theoretical methods. Since we are interested primarily in the comparison among methods, we will limit ourselves to the comparison of standard enthalpies of reaction at 298.15 K, ΔH°_{298}, for each one of the seven reactions, a property for which experimental data are readily available. These numbers are collected in Table 1.

Notice in the first place the effect of basis set extension in the results afforded by DFT methods. The most important effect is produced by the extension of the valence and diffuse part of the basis set, not by the addition of polarization functions. Extension from 6-31G(d,p) to 6-311 +G(d,p) modifies the results for different reactions by 2–3 kcal/mol. Further extension of the polarization space from (d,p) to (3df,2pd) produces a tenfold smaller effect. The maximum absolute deviation (MAD) and root mean square error (RMSE) with respect to the experimental results obtained using reported standard enthalpies of formation show for almost all methods the counterintuitive result that an improvement in the basis set actually worsens the agreement with experiment. Only in the case of the τ-dependent BMK DFT method, developed specifically for thermochemical and kinetic studies, the increase in the basis sets results in better agreement with the experiment.

All DFT methods perform as well as or better than composite model chemistries employed. In particular, the results obtained with the M06 and BMK methods, independently of the basis sets, are better than even the more elaborated post-Hartree–Fock CBS-APNO and G4 calculations, where multiple steps are combined to obtain a good estimation of correlation energy. The pure MP2

Table 1 Enthalpies of reaction (at 298.15 K, in Kcal/mol) for reactions (1)–(7)

Method	Basis[a]	(R1) $C_3H_8 \rightarrow C_2H_5\cdot + CH_3\cdot$	(R2) $C_3H_8 \rightarrow iC_3H_7\cdot + H\cdot$	(R3) $C_3H_8 \rightarrow nC_3H_7\cdot + H\cdot$	(R4) $C_3H_8 + H\cdot \rightarrow iC_3H_7\cdot + H_2$	(R5) $C_3H_8 + H\cdot \rightarrow nC_3H_7\cdot + H_2$	(R6) $C_3H_8 + CH_3\cdot \rightarrow iC_3H_7\cdot + CH_4$	(R7) $C_3H_8 + CH_3\cdot \rightarrow nC_3H_7\cdot + CH_4$	MAD	RMSE
B3LYP	I	85.5	96.9	101.1	−9.3	−5.1	−8.7	−4.5	4.2	2.5
	II	81.6	94.8	98.7	−9.7	−5.9	−8.3	−4.4	6.6	3.8
	III	81.5	94.7	98.7	−10.0	−6.0	−8.5	−4.5	6.7	3.9
B3PW91	I	86.4	95.6	99.9	−7.5	−3.3	−8.7	−4.5	3.4	2.1
	II	83.2	93.8	97.7	−7.9	−3.9	−8.3	−4.4	5.2	3.3
	III	83.0	93.7	97.7	−8.1	−4.1	−8.6	−4.6	5.3	3.5
PBE0	I	88.8	95.4	99.5	−5.1	−0.9	−8.5	−4.4	3.6	2.0
	II	85.6	93.4	97.2	−4.7	−0.8	−8.1	−4.3	5.6	3.0
	III	85.4	93.2	97.2	−4.7	−0.7	−8.4	−4.4	5.8	3.2
M06	I	90.4	97.1	101.6	−4.9	−0.4	−9.0	−4.5	3.3	2.0
	II	87.2	95.2	98.7	−4.3	−0.8	−8.4	−4.9	3.8	2.3
	III	86.2	95.2	98.7	−4.2	−0.7	−8.7	−5.1	3.8	2.4
BMK	I	92.0	98.9	102.6	−3.5	0.2	−7.5	−3.8	3.8	2.2
	II	88.4	97.2	100.6	−4.5	−1.1	−7.1	−3.7	2.1	1.2
	III	88.6	97.3	100.8	−4.6	−1.1	−7.3	−3.8	2.1	1.2
CBS-4 M		90.4	99.1	102.2	4.0	7.0	−6.3	−3.2	10.2	5.3
CBS-QB3		89.7	98.9	102.0	−0.6	2.4	−6.5	−3.4	5.6	2.8
CBS-APNO		89.7	99.1	102.1	−0.3	2.7	−6.3	−3.3	5.9	3.0
G4		88.0	97.9	100.7	0.3	3.1	−6.6	−3.8	6.3	3.2
MP2	III	92.0	97.6	100.0	−0.4	2.1	−5.0	−2.5	5.3	3.7
CCSD(T)	III	87.0	96.5	99.7	−6.4	−3.1	−6.8	−3.6	2.5	1.3
Experimental[b]		88.2 ± 0.5	99.0 ± 0.5	101.0 ± 0.5	−5.1 ± 0.5	−3.2 ± 0.5	−5.7 ± 0.5	−3.8 ± 0.5		
Other experimental[c]		88.7[d]								

Maximum absolute deviations (MAD) and root mean square errors (RMSE) calculated with respect to experimental values estimated using data in Ref. [48]

[a] Definition of the basis sets: 6-31G(d,p) (basis I), 6-311 +G(d,p) (basis II), and 6-311 ++G(3df,2pd) (basis III)

[b] Experimental values were obtained using the data in Ref. [48]

[c] Alternative experimental data were obtained from individual sources

[d] Tsang [13]

calculation, which uses a large basis set but lacks the correlation energy correction contained in the composite methods, exhibits a larger RMSE, about three times larger than the BMK RMSE, with a considerably larger computational effort. As one could expect, the CCSD(T)//MP2/6-311 ++G(3df,2pd) procedure affords values closest to the experimental data, with an RMSE of 0.9 kcal/mol. This is not significantly better than the 1.2 kcal/mol registered at the BMK level using basis sets II or III.

Thus, using this restricted set of reactions, we can conclude that BMK/6-311 ++G(3df,2pd) is the best level of calculation we can reach from the thermochemical point of view. Moreover, the use of the extended basis set is not really necessary. The results are equally good resorting to the cheaper BMK/6-311 +G(d,p) procedure, therefore, allowing the calculation of enthalpies for larger molecules.

Zheng [49] performed composite method calculations on several cracking reactions. His results are collected in Table 2, together with those obtained by us. As expected, the G4 results obtained in this paper are closer on average to the experimental results than either G2 or G3. This is particularly noticeable for the abstraction of H from the $CH_3C(CH_3)_2$ radical (eighth row in Table 2) for which a 5 kcal/mol difference with G3 makes the G4 result much nearer to the experimental enthalpy of reaction. Neither the complete basis set methods nor the CCSD(T)//MP2 procedure is able to give an accurate enthalpy of reaction for this hydrogen abstraction. In fact, all composite methods behave in a similar way. The specially designed CBS-RAD(MP2) [50] method affords worse results than CBS-QB3 and the more complete CBS-APNO method is only marginally better. All of them give results of comparable accuracy to that of CCSD(T)//MP2, including the failure in the above-mentioned dehydrogenation reaction. The much cheaper BMK/6-311 +G(d,p) DFT method results in an maximum absolute deviation and rms error similar to G4 and better than those of the other methods, with the extra advantage that it can be applied to much larger molecules. A peculiar deviation from experiment is noticed for the CCSD(T) decomposition of the ethyl radical into the

methyl radical and methylene carbene $CH_2CH_3\cdot \rightarrow :CH_2 + CH_3\cdot$. The CCSD(T)//MP2 value of 105.0 kcal/mol is approximately 6 kcal/mol larger than the experimental 98.8 kcal/mol. All the other methods, including MP2//MP2 which is not shown in the table, afford values differing less than 2 kcal/mol from experiment. This may be related to the lack of optimization of the geometry at the CCSD(T) level or a drawback of the method. Geometry optimization of the three species at the CCSD(T) level does afford the required correction, which can be linked almost completely to the better representation of the triplet CH_2 species. The agreement of CCSD(T) with experiment is now as good as usual.

Bond-breaking reactions (1)–(3) proceed without transition states. Theory and experiment agree well in this case; about 10 kcal/mol more is needed to break any of the C–H bonds than the C–C bond. Reactions (4)–(7) proceed instead through transition states. Further insight into these elementary reactions can then be obtained from the analysis of the reaction paths. Transition states were located for those reactions at the DFT and MP2 level of theory. Important geometrical parameters for these structures are shown in Fig. 2.

Transition states are more product-like when the hydrogen is abducted from the primary than from the secondary carbon, both for the abstraction by H· and $CH_3\cdot$. The structures obtained at the BMK/6-311 ++G(3df,2pd) level are in all cases looser than those obtained using the MP2 method and the same basis set. There are obviously no experimental data to compare with, but the differences among the methods are anyway small enough as to be of no substantial consequence with respect to the reaction mechanism. Abstraction reactions proceed in a simple way, as expected, and no extraordinary geometrical features are to be noticed. Barrier heights at different theoretical levels are collected in Table 3.

There are in these cases several sources of experimental data. The more consistent energies of activation for the direct and reverse reactions are those of Tsang [13], who reassessed previous experimental work and fitted modified Arrhenius equations in most cases. Nonetheless, we have considered also the other experimentally derived Arrhenius data for the direct reactions. In this case, all temperature dependence is built only in the exponential part. Therefore, the activation energies are larger than the exponential factors in Tsang results. Errors in the activation energies are higher than the ones for the enthalpies of reaction. In all cases, the theoretically derived energies of activation agree worse with Tsang values than with those from other sources. The influence of the inclusion of higher levels of correlation on the activation energy is quite obvious, comparing for instance the G4 values for reaction (4) to the MP2 ones. Results obtained using BMK are not in this case better than those obtained with other DFT methods, M06 being the best method overall, judging from the agreement with the experimental data available. Differences among methods are not so important, however, as to prefer definitely one over the other.

Since the four reaction paths involve proton transfers, it is possible that the disagreement between the theoretical and experimental data may be explained by tunneling effects. Moreover, the temperature dependence of the preexponential factor may be also a cause for the discrepancies between theoretical and experimental data. Therefore, we calculated the parameters in the Arrhenius and modified Arrhenius equations for the forward reactions using the BMK/6-311 ++G(3df,2pd) method and the Eckart correction for tunneling. They are collected in Table 4.

The activation energies are in reasonable agreement with the experimental data for Arrhenius equations. The preexponential factors, however, are not so good. A better agreement is obtained with the modified Arrhenius equation. Now, the preexponential factors and temperature dependence are reasonable, and activation energies are not far from experimental value (MADs are under 1 kcal/mol). From a kinetic point of view, however, the description is semiquantitative at best. If one plots the rate constants obtained theoretically and experimentally for these reactions, the picture shown in Fig. 3 is obtained. There is a quite a difference between experimental and theoretical data at each temperature, which could be adjusted by a simple multiplicative factor for each reaction. The calculations predict that the ratio of formation of the 1-propyl radical to the 2-propyl radical would be about 5 times faster theoretically than observed experimentally. Both theoretically and experimentally, one observes that increase in the temperature equalizes the rate of formation of both radicals, but experimentally this happens faster than what the theoretical calculations predict. This failure is not corrected even considering internal rotation to perform more precise thermochemical calculations.

3.2 Propyl radicals

Reactions (2)–(7) have in common the production of the two isomers of the propyl radical, *i*-propyl, **2,** and *n*-propyl, **3**. About 100 kcal/mol is necessary to obtain these products by hydrogen loss through reactions (2) and (3), without transition states. Reaction (1) requires about 12 kcal/mol less energy and should then proceed faster. However, after the methyl radicals start to accumulate in the reactor because of reaction (1), hydrogen abstraction through reactions (6) and (7) become more favorable, due to an activation energy of only about 10 kcal/mol. The process would lead then to the emergence of $C_2H_5\cdot$ and the propyl radicals, which would later react further.

Table 2 Comparison of computed enthalpies of reaction (at 298.15 K, in Kcal/mol, kcal/mol) for reactions in Ref. [49]

Reaction	G2[a]	G3[a]	G4[b]	CBS-QB3[a]	CBS-RAD(MP2)[a]	CBS-APNO[b]	BMK[b,c]	CCSD(T)//MP2[d]	Exp.[e]
$\cdot CH_2CH_3 \rightarrow CH_2CH_2 + H\cdot$	33.63	34.51	35.90	35.00	34.17	36.36	37.43	36.16	36.24
$CH_3CH_3 \rightarrow \cdot CH_2CH_3 + H\cdot$	101.34	99.65	100.68	100.20	100.49	101.80	100.25	99.40	100.50
$CH_3CH_2CH_2 \rightarrow CH_3CH\cdot CH_2 + H\cdot$	30.73	31.58	34.50	31.08	31.33	32.58	34.08	33.33	33.08
$CH_3CH\cdot CH_3 \rightarrow CH_3CHCH_2 + H\cdot$	33.67	34.25	37.33	34.56	34.31	35.58	37.48	36.58	34.98
$CH_3CH_2CH_3 \rightarrow \cdot CH_2CH_2CH_3 + H\cdot$	101.77	100.40	100.68	101.43	101.02	102.13	100.61	99.73	101.02
$CH_3CH_2CH_2CH_3 \rightarrow \cdot CH_2CH_2CH_2CH_3 + H\cdot$	103.63	99.99	100.65	100.94	100.69	102.29	101.01		101.56
$CH_3CH_2CH_2CH_3 \rightarrow CH_3CH\cdot CH_2CH_3 + H\cdot$	99.06	97.63	97.83	98.17	98.16	99.40	97.45		98.13
$CH_3C(CH_3)_2 \rightarrow \cdot CH_2C(CH_3)_2 + H\cdot$	33.77	34.20	39.67	34.51	34.43	34.88	40.75		41.10
$\cdot CH_2CH_3 \rightarrow CH_2 + \cdot CH_3$	98.69	97.49	99.05	100.79	98.53	100.27	99.92	105.04 (97.34)	98.77
$\cdot CH_2CH_2CH_3 \rightarrow CH_2CH_2 + \cdot CH_3$	24.21	20.96	23.19	22.77	21.76	23.97	25.25	23.42	23.46
$\cdot CH_2CH_2CH_2CH_3 \rightarrow CH_2CH_2 + \cdot CH_2CH_3$	21.25	21.10	22.36	21.85	22.16	22.95	22.83		21.67
$\cdot CH_2CH(CH_3)_2 \rightarrow \cdot CH_3 + CH_3CHCH_2$	19.27	20.19	23.86	22.21	21.20	22.14	23.14		22.70
$CH_3CH\cdot CH_2CH_3 \rightarrow \cdot CH_3 + CH_3CHCH_2$	21.30	21.05	24.82	23.43	22.32	23.34	25.29		23.70
Maximum absolute deviation	7.33	6.90	2.30	6.59	6.67	6.22	2.50	6.27 (1.60)	
Root mean square error	2.67	2.46	1.04	2.05	2.16	1.94	1.19	2.53 (1.04)	

MADs and RMSEs have been recalculated for the data present in Ref. [49], taking into account the experimental data in Ref. [48]

[a] From Ref. [49]

[b] This work

[c] BMK/6-311 +G(d,p)

[d] Values in parenthesis are calculated at the CCSD(T)//CCSD(T)/6-311 ++G(3df,2pd) level

[e] Experimental results taken from Ref. [48], except for $CH_2CH_2CH_2CH_3$; in this case, data from Ref. [49] were taken instead

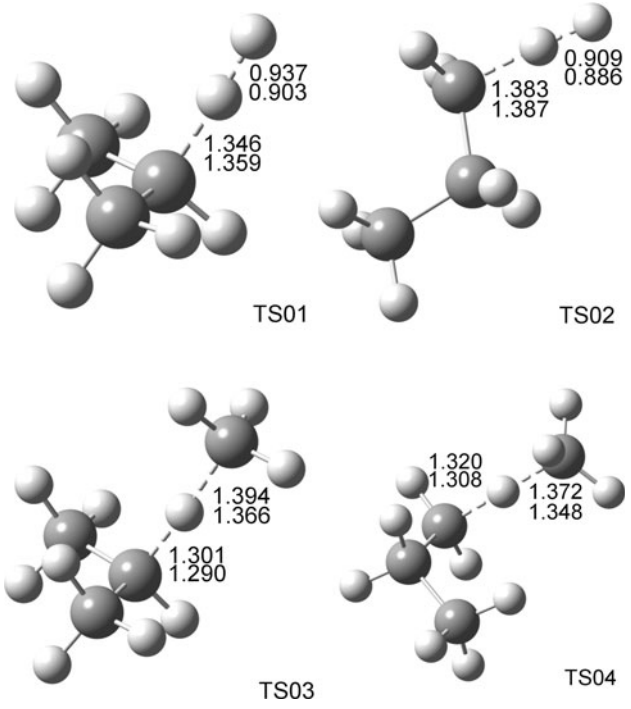

Fig. 2 Structure of the transition states for reactions (4)–(7), TS01 to TS04, respectively. Some important bond distances are shown. The upper entries correspond to BMK calculations, while the lower entries correspond to MP2 calculations. The 6-311 ++G(3df,2pd) basis set was employed in both cases. Distances are expressed in Å

Direct interconversion of the propyl radical isomers is not an easy step. The transition state for reaction (8) involves a three-atom 1,2-hydrogen transfer whose transition states TS05 are shown in Fig. 4.

$$iC_3H_7 \cdot (\mathbf{2}) \leftrightarrows nC_3H_7 \cdot (\mathbf{3}) \quad (8)$$

The barrier for this reaction is about 41 kcal/mol at room temperature (all methods agree to within one kcal/mol), but easy to overcome at the temperatures at which the more energy-consuming C–C or C–H bond breakings in propane take place. In a previous study of this reaction published by Matheu et al. [53], they derived the expression $k(T)\ s^{-1} = 5.36 \times 10^{12}\ T^{0.88}\ \exp(-30.13/RT)$ with the temperature expressed in K and the exponential factor in kcal/mol. From our own BMK/6-311 ++G(3df,2pd), we obtained a somewhat similar expression $k(T)\ s^{-1} = 5.35 \times 10^{12}\ T^{0.86}\ \exp(-46.82/RT)$ with a 50 % higher activation energy. The presence of propane lowers the barrier, according to experimental data by Berkley et al. [54], but we did not calculate the corresponding transition state, since even in the most unfavorably hypothesis, the equilibrium would be established without difficulties.

As would be expected, **2** is more stable than **3** because of a better stabilization of the unpaired electron. Papic and Laidler [14, 15] determined the energy difference between these isomers as −3.5 kcal/mol in the seventies. More recent work by Tsang in 1996 gauged the enthalpy

Table 3 Energies of activation for reactions (4)–(7) in kcal/mol

Reaction		B3LYP[a]	B3PW91[a]	PBE0[a]	M06[a]	BMK[a]	MP2[a]	CBS			G4	Experimental
								4 M	QB3	APNO		
(4)	$C_3H_8 + H\cdot \rightarrow iC_3H_7\cdot + H_2$	2.4	3.5	4.3	6.7	8.5	12.6	8.3	7.4	7.0	7.3	7.96[b], 4.47[c]
	$iC_3H_7\cdot + H_2 \rightarrow C_3H_8 + H\cdot$	13.4	12.6	11.0	14.9	14.2	14.0	15.0	14.8	13.4	14.9	8.67[c]
(5)	$C_3H_8 + H\cdot \rightarrow nC_3H_7\cdot + H_2$	5.3	6.6	7.6	8.7	11.5	15.6	11.3	10.3	9.9	10.3	9.37[b], 6.76[c]
	$nC_3H_7\cdot + H_2 \rightarrow C_3H_8 + H\cdot$	12.1	11.6	10.2	12.6	13.3	14.4	14.7	14.5	13.2	15.0	9.13[c]
(6)	$C_3H_8 + CH_3\cdot \rightarrow iC_3H_7\cdot + CH_4$	9.2	10.2	9.0	10.2	11.5	11.9	11.7	11.5	11.2	11.9	9.60[d], 5.48[c]
	$iC_3H_7\cdot + CH_4 \rightarrow C_3H_8 + CH_3\cdot$	18.1	19.0	17.6	19.2	19.1	17.2	18.2	18.3	17.6	18.8	10.80[c]
(7)	$C_3H_8 + CH_3\cdot \rightarrow nC_3H_7\cdot + CH_4$	12.2	12.4	11.2	13.2	14.5	15.6	14.2	13.9	13.4	14.2	11.50[d], 7.15[c]
	$nC_3H_7\cdot + CH_4 \rightarrow C_3H_8 + CH_3\cdot$	17.7	17.1	15.8	18.0	18.3	18.2	17.5	17.4	16.7	18.1	10.87[c]
MAD[e]		5.6/8.7	4.5/8.2	3.6/6.8	1.7/8.4	3.0/8.3	6.3/8.7	2.7/7.4	2.4/7.5	1.9/6.8	2.7/8.0	
RMSE[f]		3.5/5.0	2.7/4.7	2.0/3.6	1.1/5.4	2.1/6.1	4.5/7.1	2.0/6.0	1.6/5.8	1.3/5.1	1.9/6.1	

[a] Calculated in this using the 6-311 ++G(3df,2pd) basis set, at 1 atm and 298.15 K

[b] Baldin and Walker [51], 300–753 K

[c] Tsang [13] recommended value, 400–900 K

[d] Kerr and Parsonage [52], 550–750 K

[e] First entries are the MADs for the four direct reactions considering the experimental data from Refs. [51] and [52], and second entries are MADs for the eight direct and reverse reactions with respect to the experimental data in Ref. [13]

[f] First entries are the RMSEs for the four direct reactions considering the experimental data from Refs. [51] and [52], and second entries are RMSEs for the eight direct and reverse reactions with respect to the experimental data in Ref. [13]

Table 4 Comparison of theoretical and experimental Arrhenius and modified Arrhenius parameters

Reaction		Theoretical[a]		Experimental[a,b]		Theoretical[a,c]	Experimental[a,c,d]
		A	E	A	E		
(4)	$C_3H_8 + H\cdot \rightarrow iC_3H_7\cdot + H_2$	4.98×10^6	7.09	9.76×10^7	7.96	$3.63 \times 10^4 (T/T_{ref})^{3.7} \exp(-4.15/RT)$	$1.13 \times 10^4 (T/T_{ref})^{2.40} \exp(-4.47/RT)$
(5)	$C_3H_8 + H\cdot \rightarrow nC_3H_7\cdot + H_2$	3.95×10^6	9.77	1.32×10^6	9.38	$3.72 \times 10^4 (T/T_{ref})^{3.6} \exp(-7.03/RT)$	$2.55 \times 10^4 (T/T_{ref})^{2.54} \exp(-6.76/RT)$
(6)	$C_3H_8 + CH_3\cdot \rightarrow iC_3H_7\cdot + CH_4$	1.62×10^7	11.11	1.99×10^5	9.61	$1.04 \times 10^3 (T/T_{ref})^{7.4} \exp(-5.41/RT)$	$5.48 \times 10^0 (T/T_{ref})^{3.46} \exp(-5.48/RT)$
				8.57×10^4	13.25		
(7)	$C_3H_8 + CH_3\cdot \rightarrow nC_3H_7\cdot + CH_4$	2.91×10^6	12.49	1.01×10^4	11.74	$1.70 \times 10^2 (T/T_{ref})^{7.6} \exp(-6.80/RT)$	$9.71 \times 10^0 (T/T_{ref})^{3.65} \exp(-7.15/RT)$
				4.52×10^5	14.92		
				4.37×10^4	17.51		

Theoretical calculations were performed using the BMK/6-311 ++G(3df,2pd) method including the Eckhart tunneling correction

[a] Preexponential factors in $m^3mol^{-1}s^{-1}$, activation energies in kcal/mol, $T_{ref} = 298$ K, T in K

[b] Data from Refs. [51], [52], [57] and [64]

[c] Preexponential factors in $m^3molecule^{-1}s^{-1}$, and exponential parameters in kcal/mol

[d] Data from Ref. [13]

difference at room temperature at -1.9 ± 1.0 kcal/mol [5]. Our own values at several theoretical levels are collected in Table 5. The best calculated results (BMK/6-311 ++G(3df,2pd), CBS-QB3, CBS-APNO) give a lower value, which can be expressed as -3.0 ± 0.5 kcal/mol.

The two isomers of the propyl radical can react with themselves or each other, in the following chain termination reactions

$$nC_3H_7\cdot(\mathbf{3}) + nC_3H_7\cdot(\mathbf{3}) \rightarrow nC_6H_{14}(\mathbf{5}) \quad (9a)$$

$$nC_3H_7\cdot(\mathbf{3}) + nC_3H_7\cdot(\mathbf{3}) \rightarrow C_3H_8(\mathbf{1}) + C_3H_6(\mathbf{12}) \quad (9b)$$

$$iC_3H_7\cdot(\mathbf{2}) + iC_3H_7\cdot(\mathbf{2}) \rightarrow (CH_3)_2CHCH(CH_3)_2(\mathbf{4}) \quad (10a)$$

$$iC_3H_7\cdot(\mathbf{2}) + iC_3H_7\cdot(\mathbf{2}) \rightarrow C_3H_8 + C_3H_6(\mathbf{12}) \quad (10b)$$

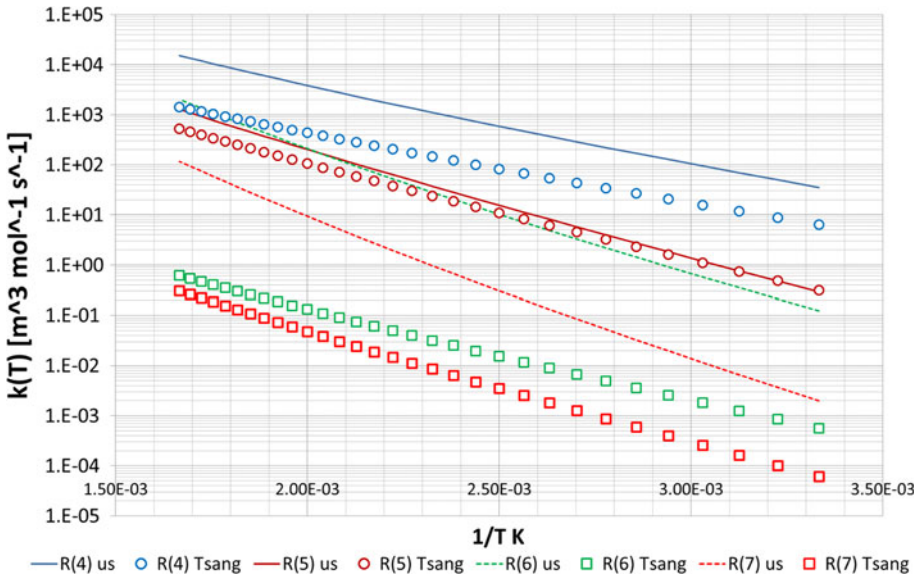

Fig. 3 Variation of the rate of reactions (4)–(7) with the inverse of the temperature, plotted in a logarithmic scale. *Circles* and *squares* identify fitted experimental data for hydrogen abstraction by the H and CH_3 radicals, respectively. *Lines* represent the theoretical data. Reactions are *color coded*, using the same color for the experimental and theoretical data

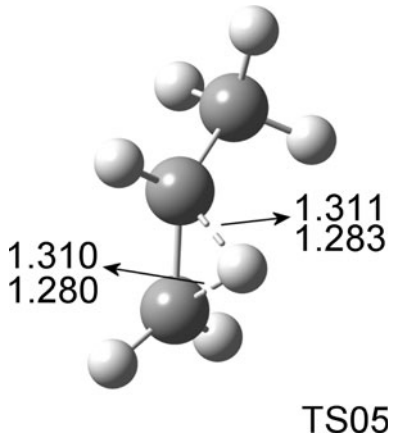

Fig. 4 Transition state TS05 for the interconversion between the *i*-propyl and *n*-propyl radicals

$$iC_3H_7 \cdot (\mathbf{2}) + nC_3H_7 \cdot (\mathbf{3}) \rightarrow (CH_3)_2CH(CH_2)_2CH_3(\mathbf{6}) \quad (11a)$$

$$iC_3H_7 \cdot (\mathbf{2}) + nC_3H_7 \cdot (\mathbf{3}) \rightarrow C_3H_8 + C_3H_6(\mathbf{12}) \quad (11b)$$

Experimental evidence for the existence of species **4–6** was found by Papic and Laidler [14, 15] who experimentally identified them as minor products for this reaction. Enthalpies in Table 5 show that reactions (9a)-(11a) liberate approximately the same energy that is required to produce C–C scission in propane, a fact that would help the reaction to proceed further. These are spontaneous reactions according to the free energy change and proceed without transition states.

Reactions (9b)-(11b) are somehow more difficult to treat. In this case, the two doublet species have to position with respect to each other in the collision complex in such a way their radical centers are separated, least they will end up giving the same products as in reactions (9a)-(11a). They can couple to form either a singlet or a triplet state complex, but the first one would be preferred since the final species are in their ground, closed-shell singlet states. Reaction in these cases would proceed through a hydrogen atom transfer like in the case of reactions (4)–(7). However, in this case, we have two radicals whose internal structures rearrange during the transfer. A electron density redistribution is produced in both participating monomers, due to the pairing of the preexisting lone electron with the one newly formed after H-atom transfer.

The correct treatment of such an open-shell complex should be performed using a multireference wave function. However, less accurate methods can give an idea of the structure of the complex. A semiempirical PM3 geometry optimization was first attempted for the complex between *n*-propyl and *i*-propyl radicals. The process converged toward a structure shown in Fig. 5a where it is very clear how the carbons bearing the lone electrons avoid each other. The spin distribution of this open-shell singlet state, Fig. 5c, shows the presence of one electron with alpha spin and one with beta spin localized on the primary and secondary carbons of each fragment, respectively. A single point BMK calculation was performed on this complex at the PM3 geometry using the larger basis sets, and the spin distribution of the singlet open shell is shown in Fig. 5d. It is similar to the PM3 spin distribution, only that the p-character of the orbitals is less marked. The open-shell singlet radical calculated at the DFT level is heavily spin-contaminated by the triplet, $\langle S^2 \rangle = 1.00$, $S = 0.61$, which is about 0.4 kcal/mol less stable. As must be obvious, a closed-shell calculation using this geometry lies at much higher energies (about 39 kcal/mol over the open-shell singlet).

Table 5 Reaction enthalpies calculated at 298.15 K for reactions 8 to 11a, 11b in this work compared to experimental results

Method	Basis	R8	R9a	R9b	R10a	R10b	R11a	R11b	MAD	RMSE
B3LYP	I	−4.2	−82.7	−63.5	−73.0	−55.1	−78.3	−59.3	13.5	8.0
	II	−3.9	−78.7	−63.1	−69.7	−55.3	−74.7	−59.2	16.8	9.9
	III	−4.0	−78.4	−63.5	−69.2	−55.5	−74.3	−59.5	17.3	10.0
B3PW91	I	−4.2	−83.6	−61.7	−73.9	−53.2	−79.2	−57.4	12.5	8.3
	II	−3.9	−80.4	−61.3	−71.5	−53.4	−76.4	−57.3	15.0	9.6
	III	−4.0	−80.1	−61.5	−71.0	−53.4	−76.0	−57.5	15.5	9.8
PBE0	I	−4.2	−86.5	−60.7	−77.8	−52.4	−82.6	−56.6	11.7	7.4
	II	−3.9	−83.2	−60.3	−75.4	−52.6	−79.8	−56.4	11.6	8.4
	III	−3.9	−83.0	−60.5	−74.8	−52.6	−79.4	−56.6	11.7	8.5
M06	I	−4.5	−89.0	−63.8	−81.8	−54.8	−85.9	−59.3	9.3	5.1
	II	−3.5	−84.4	−62.0	−79.3	−55.0	−82.4	−58.5	9.2	6.2
	III	−3.6	−83.9	−62.2	−78.5	−55.0	−81.6	−58.6	9.1	6.4
BMK	I	−3.7	−90.4	−67.0	−83.3	−59.5	−87.2	−63.2	4.6	2.7
	II	−3.4	−86.7	−66.5	−80.5	−59.7	−83.9	−63.1	6.0	3.4
	III	−3.5	−86.8	−67.2	−81.3	−60.2	−83.8	−63.7	5.2	3.1
CBS-4 M		−3.1	−90.3	−67.4	−86.0	−61.3	−88.6	−64.3	2.9	1.7
CBS-QB3		−3.0	−89.6	−68.1	−85.6	−62.0	−87.9	−65.1	2.1	1.3
CBS-APNO		−3.0	−89.7	−69.5	−85.6	−63.5	−88.1	−66.5	2.0	1.2
G4		−2.8	−87.5	−66.2	−84.0	−60.5	−86.1	−63.4	3.6	2.2
MP2	III	−2.5		−70.8		−65.9		−68.3	2.9	2.1
CCSD(T)	III	−3.3		−66.4		−59.9		−63.1	4.3	2.8
Experimental		−1.9 ± 1.0	−87.7 ± 1.0	−67.9 ± 1.0	−86.5 ± 1.0	−64.1 ± 1.0	−87.6 ± 1.0	−66.0 ± 1.0		
		−3.5								

Enthalpies in kcal/mol

No transition state was located for these reactions at the DFT level. Geometry optimizations using the BMK functional with either the medium or large basis sets led to the transfer of a hydrogen atom, H14 in Fig. 5, giving the optimum structure depicted in Fig. 5b. However, a priori one could not rule out the possibility of a conical intersection between the open-shell and closed-shell singlet potential energy surfaces. Multireference calculations, outside the scope of this paper, should be performed to rule out this path. However, this avenue of research was not pursued further in this paper because the thermochemistry of reactions (9b)-(11b) shows that they are less favorable than reactions (9a)-(11a) and less exothermic. Therefore, although these (b) channels might be open, they are anyhow probably less important than the (a) channels, the result of head-on collision of the radical centers in each one of the molecules.

3.3 β-scission reaction

An important difference between isomers **2** and **3** of the propyl radical is that the latter can produce ethylene and the methyl radical, which would increase the concentration of this species, arising from reaction (1). The process is known as a β-scission reaction and in the case of the propyl radical is represented by reaction (12)

$$nC_3H_7\cdot(\mathbf{3}) \rightarrow C_2H_4(\mathbf{8}) + CH_3\cdot \qquad (12)$$

This reaction has been studied experimentally by Bencsura et al. [12] and theoretically using G3 and CBS models by Zheng and Blowers [8]. A drawback of this latter theoretical study is that the geometry optimization necessary to obtain the transition state was performed at the low MP2/6-31G(d) level. As shown in Fig. 6, the structure varies considerably when better levels of theory are applied. In particular, MP2 calculations tend to give a too tight transition state, while BMK and other DFT methods give a looser, more product-like transition state. Therefore, the barriers obtained with MP2 are higher than those obtained with DFT methods. To an extent, the drawback of the MP2 method is partially corrected by error compensation when a small basis set is used as in [8]. Higher levels of correlation energy, as added in G3 or CBS methods, may help correct this high activation energies obtained at the MP2 level.

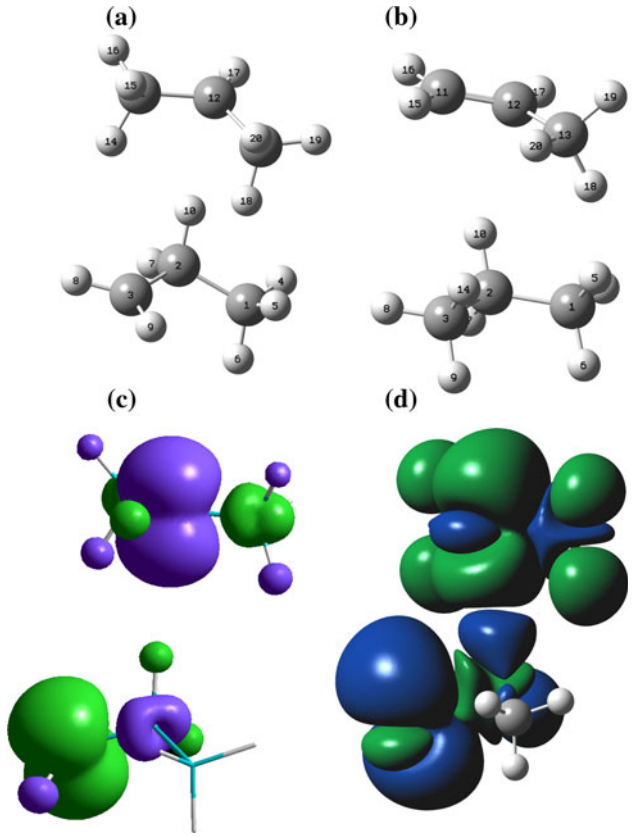

Fig. 5 **a** Optimum structure of the complex between *i*-propyl and *n*-propyl radicals, obtained at the semiempirical PM3 level of theory; **b** final optimized structure obtained at the DFT BMK/6-311 +G(d,p) level starting from the optimum PM3 geometry; **c** PM3 spin density at the PM3 optimum structure; **d** DFT BMK/6-311 +G(d,p) spin density at the PM3 optimum geometrical structure

Enthalpies of reaction and activation energies at room temperature are collected for several theoretical levels of calculation in Table 6 and compared to the experimental data available. With respect to the heat of reaction, DFT methods are reasonably close, in general, but tend to be outside the error bars of the experimental determination, except in the case of B3PW91 and BMK. Basis set extension is provoking a noticeable effect in the same way as mentioned before. BMK calculations with the more extended basis sets gave an enthalpy of reaction similar to that afforded by the CBS-4M or MP2 methods, while the other CBS and G4 composite methods are nearer to experiment. As expected, the CCSD(T) result is the nearest to the experimental value.

Thermal corrections are important, as one can see from the difference between the zero point-corrected energy barriers and the enthalpy barriers at 298 K. The barriers are in general several kcal/mol larger than the experimental activation energies reported in the literature, proportionally more significant for the reverse than for the forward reaction. To make a precise comparison, however, it is necessary to try two- and three-parameter Arrhenius fits and include corrections for tunneling and hindered internal rotations. The results obtained using the BMK method with the large basis set between 600 and 1,000 K, including tunneling and hindered rotor corrections, are shown in Table 7.

The agreement between the activation energies for both the forward and reverse reactions using the generalized Arrhenius equation is very good. Preexponential factors depend on the temperature in both cases, but the effect is more marked in the case of the reverse equation. A two-parameter Arrhenius equation does not represent well the curvature of k(T) with respect to T, and therefore, the activation energy is about 40 % too large. The extended Arrhenius parameters calculated at the BMK/6-311 ++G(3df,2pd) level are, however, in excellent agreement with the experimental results. Tunneling does not contribute markedly to the barrier, as expected, but internal rotation in both the *n*-propyl radical and the transition state does. Calculations were not repeated with the CBS, G3, or G4 methods, but it is to be expected that activation energies calculated with them will be too small, since the energy barriers are already in the same range as the experimentally observed activation energies.

3.4 Chain initiation reactions

Reactions (1)–(3) are not the only possible initiation elementary steps. Lower molecular weight hydrocarbons, like methane, ethane, ethene and propene, as well as higher molecular weight species are produced, as shown in Fig. 1. It is highly unlikely that higher molecular weight species are available in large enough concentrations to contribute

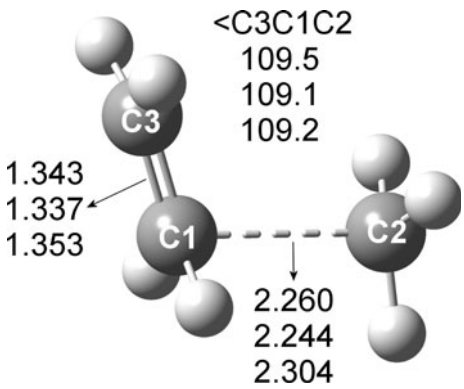

Fig. 6 Transition state TS06 for the β-scission reaction. Bond lengths in Å and bond angle in degrees. First entry corresponds to MP2/6-31G(d) optimization in Ref. [8], and second and third entries correspond to MP2 and BMK calculations using the 6-311 ++G(3df,2pd) basis set performed in this work

Table 6 Energy characterization of the β-scission reaction

Method	Basis	ΔH^{o}_{react}	$\Delta H^{\#}_{direct}$	$\Delta H^{\#}_{inverse}$	Energy barrier (direct reaction)	Energy barrier (inverse reaction)
B3LYP	I	24.8	30.2	5.5	34.3	6.6
	II	20.9	28.0	7.1	31.9	8.2
	III	20.4	27.7	7.3	31.7	8.4
B3PW91	I	27.6	33.1	5.5	37.2	6.6
	II	24.6	31.3	6.7	35.2	7.8
	III	24.2	31.0	6.8	35.0	7.9
PBE0	I	30.9	35.0	4.1	39.1	5.2
	II	27.8	33.2	5.4	37.0	6.5
	III	27.5	33.0	5.5	36.8	6.6
M06	I	29.3	32.9	3.5	37.2	4.8
	II	26.7	31.5	4.8	35.0	6.0
	III	26.2	31.3	5.1	34.9	4.0
BMK	I	28.7	35.0	6.3	38.7	7.4
	II	25.2	32.9	7.6	36.3	8.7
	III	24.9	32.7	7.8	36.2 [33.8][15]	9.0 [6.88][15]
CBS-4 M		24.9	30.6	5.8	30.5	7.0
CBS-QB3		23.2	29.4	6.2	29.2	7.3
CBS-APNO		24.0	30.3	6.4	30.2	7.6
G4		23.2	30.4	7.2	30.2	8.3
MP2	III	24.5	39.2	14.6	42.2	19.1
CCSD(T)	III	23.4				
Zheng G3[1]		20.0			30.0	10.0
Zheng CBS[1]		21.2			29.6	8.4
Other Theoretical					31.43[10], 30.07[10]	11.11[10], 7.43[10]
Experimental[16]		23.5 ± 1.0[2]			30.40[3], 32.99[4], 27.82[5], 32.59[6], 32.59[7], 31.40[8], 34.58[9]	7.89[6], 7.83[11], 7.35[12], 7.71[13,14]

Energies in kcal/mol

[1] Ref. [49, 50]; [2] Ref. [48]; [3] Ref. [55]; [4] Ref. [56]; [5] Ref. [57]; [6] Ref. [58]; [7] Ref. [15]; [8] Ref. [59]; [9] Ref. [60]; [10] CBS-QB3 Ref. [61]; [11] Ref. [62]; [12] Ref. [63]; [13] Ref. [52]; [14] Ref. [5]; [15] Values in brackets are energies of activation, see text..

[16] Experimental heat of reaction and energies of activation

Table 7 Energies of activation in kcal/mol obtained at the BMK/6-311 ++G(3df,2pd) level compared to experimental data

Method	E + ZPE Barrier	Two-parameter Arrhenius equation[a]			Three-parameter Arrhenius Equation[b]	Experimental
		Without corrections	Tunneling Correction	Tunneling + Hindered Rotation		
Direct reaction	36.2	34.4	34.3	33.8	31.8 ($n = 1.17$)	30.46 ($n = 0.87$)[c]
Reverse reaction	9.0	13.7	13.6	10.6	6.88 ($n = 2.43$)	6.13 ($n = 2.48$)[c]

[a] Expressed as A $\exp(-E_a/RT)$; [b] expressed as A $(T/298)^n \exp(-E_a/RT)$; [c] Ref. [9]

significantly to the mechanism. But it cannot be excluded that the simpler hydrocarbons do decompose at a similar or larger rate than propane, a question to be investigated in this section of the paper.

Eleven chain initiation reactions were considered in this paper. On one side, we have reactions (1)–(3) described previously for propane. In addition, we have also the following eight reactions

$$C_3H_6(\mathbf{12}) \rightarrow CH_2 = CHCH_2 \cdot (\mathbf{13}) + H\cdot \quad (13a)$$

$$C_3H_6(\mathbf{12}) \rightarrow CH_2C \cdot CH_3(\mathbf{17}) + H\cdot \quad (13b)$$

$$C_3H_6(\mathbf{12}) \rightarrow \cdot CH = CHCH3(\mathbf{21}) + H\cdot \quad (13c)$$

$$C_3H_6(\mathbf{12}) \rightarrow C_2H_3 \cdot (\mathbf{25}) + CH_3\cdot \quad (14)$$

$$C_2H_6(\mathbf{11}) \rightarrow C_2H_5 \cdot (\mathbf{7}) + H\cdot \quad (15)$$

$$C_2H_6(\mathbf{11}) \rightarrow CH_3 \cdot + CH_3\cdot \quad (16)$$

$$C_2H_4(\mathbf{8}) \rightarrow C_2H_3 \cdot (\mathbf{25}) + H\cdot \quad (17)$$

$$CH_4 \rightarrow CH_3 \cdot + H\cdot \quad (18)$$

Bold numbers identify the species in the global reaction mechanism depicted in Fig. 1. All of them occur without identifiable transition states, and the comparison among theoretical and experimental results is shown in Table 8. In this initiation reactions appear the H· and CH_3· radicals, as in reactions (1)–(3), but also other small radicals that can participate in chain elongation reactions, namely C_2H_3·, C_2H_5·, and different isomers of C_3H_5·.

The results for the CCSD(T) method are very good, as expected. The computed values are within the experimental error margins. CBS-APNO results are as good or better than the CCSD(T). In both cases, the results are not completely coherent because the optimization of geometry and the different contributions to the correlation energy are calculated using different methods. BMK results with the extended basis, on the contrary, are as good as either of the former, while now the geometry optimization as well as the calculation of all the energies and derivatives is performed at the same computational level.

According to the BMK results, reactions (13a), the generation of the propenyl radical, and (16), the cracking of ethane, occur at temperatures comparable to those necessary for the cracking of propane. Propene and ethane are both generated along the reaction path and are, therefore, not additional starting points. They just add to the full mechanism to proceed further toward products.

3.5 Chain propagation reactions

Reactions (4)–(8) and (12) are chain propagation reactions, where a new radical species is formed from an already existing one, adding to the pool of radicals present in the combustion chamber. Reaction of any of the radicals with any of the neutral molecules present in the reactor give either a new species or one already present from other branches of the reaction scheme. The reactions considered in this paper are shown in Table 9, where the values of the enthalpies of reaction obtained at each level with the largest basis set are reported. Experimental values, as well as MADs and RMSEs, are also included in the table.

About two-thirds of the propagation reactions in the table are exothermic, and one-third thermoneutral or endothermic. In all cases, the energy needed is much lower than the one necessary to initiate the chain of reactions. Again as before, BMK results are of comparable quality to G4 or CCSD(T), although the CBS-APNO calculations exhibit smaller deviations from the experimental values for this set of reactions. Needless to stress, the BMK calculations are faster and cheaper than the composite or coupled cluster methods, especially when larger molecules are considered.

3.6 Termination reactions

Reactions (9a), (9b)–(11a), and (11b) are termination reactions. Several more can be written, and some of them are collected in Table 10. Some of the experimental results are not available for these reactions. Thus, the theoretical values should be taken as estimates of the enthalpies of reaction.

The main difficulty in representing these reactions is that they are neither isodesmic nor isogyric. Errors do not compensate then, and only an equally accurate description of the radicals and the neutral molecules afford reasonable values for the reactions. As observed in the table, B3LYP is nearly useless for the description, since errors up to 17 kcal/mol occur. The BMK method exhibits both a MAD and RMSE of almost one-fourth those of B3LYP. The results are comparable to G4 and better than MP2, but not as good as CCSD(T) or CBS-APNO.

4 Discussion

Let us assume that the combustion takes place at a temperature where reaction (1) is feasible, but not (2) or (3). Since about 88 kcal/mol is needed to break the CC bond, there will be also enough energy to overcome the barriers of reactions (6) and (7). Therefore, once there are enough methyl radicals in the system, an equilibrium between the *n*-propyl, *i*-propyl, ethyl and methyl radicals will exist.

The calculations shown in this paper do not present any noticeable discrepancy with the known experimental values. Therefore, it is inmaterial whether the whole kinetic system is solved resorting to one type of data or the other. One could deduce from the BMK values of the energies for the reactions that the main processes can be schematized as in Fig. 7. The main products, therefore, will be methane, ethene, *n*-butane, and *i*-butane, which can in turn react forward in other chain reactions. The reduced mechanism presented in Fig. 7 amounts to the global reaction

Table 8 Comparison between theoretical and experimental enthalpies of reaction for chain initiation reactions, in kcal/mol

Method	Basis	R1	R2	R3	R13a	R13b	R13c	R14	R15	R16	R17	R18	MAD	RMSE
B3LYP	I	85.5	96.9	101.1	84.2	104.5	109.7	97.1	100.8	88.6	109.9	105.5	3.9	1.3
	II	81.6	94.8	98.7	82.6	102.9	108.0	93.5	98.5	84.5	108.1	103.1	7.5	2.0
	III	81.5	94.7	98.7	82.6	103.0	108.2	93.5	98.5	84.5	108.3	103.3	7.4	2.0
B3PW91	I	86.4	95.6	99.9	83.5	103.2	108.5	98.0	99.6	89.6	108.6	104.4	4.7	1.4
	II	83.2	93.8	97.7	82.0	101.7	106.9	95.1	97.5	86.2	107.0	102.1	6.1	2.1
	III	83.0	93.7	97.7	82.0	101.7	107.0	95.1	97.5	86.0	107.1	102.2	6.1	2.1
PBE0	I	88.8	95.4	99.5	83.1	102.9	108.1	100.3	99.2	91.7	108.2	103.9	5.1	1.4
	II	85.6	93.4	97.2	81.5	101.3	106.4	97.4	97.0	88.2	106.5	101.5	6.6	2.0
	III	85.4	93.2	97.2	81.4	101.2	106.5	97.3	96.9	88.1	106.5	101.6	6.7	2.0
M06	I	90.4	97.1	101.6	85.0	103.9	109.0	100.5	101.1	93.1	109.0	106.1	3.5	1.3
	II	87.2	95.2	98.7	83.5	102.3	107.4	97.4	99.0	89.4	107.3	103.6	4.6	1.6
	III	86.2	95.2	98.7	83.5	102.4	107.5	97.2	98.4	89.2	107.6	103.8	4.6	1.6
BMK	I	92.0	98.9	102.6	87.6	107.2	111.9	103.9	102.2	94.1	110.8	106.4	4.4	1.4
	II	88.4	97.2	100.6	86.1	105.9	110.6	100.6	100.2	90.3	109.4	104.3	2.0	0.9
	III	88.6	97.3	100.8	86.3	106.2	110.9	101.0	100.5	90.6	109.7	104.6	1.8	0.8
CBS-4 M		90.4	99.1	102.2	84.9	106.2	110.5	101.0	101.8	91.4	111.0	105.4	3.3	1.1
CBS-QB3		89.7	98.9	102.0	85.9	106.2	110.4	100.0	101.7	90.7	110.6	105.4	2.3	1.1
CBS-APNO		89.7	99.1	102.1	88.2	108.8	112.9	102.5	101.8	90.7	111.1	105.4	1.6	0.9
G4		88.0	97.9	100.7	85.8	105.4	109.5	98.6	100.7	89.0	110.0	104.5	2.4	1.0
MP2	III	92.0	97.6	100.0	91.9			110.0	99.6	91.9	114.7	102.5	9.1	4.0
CCSD(T)	III	87.0	96.5	99.7	87.4			100.8	99.4	88.1	110.7	103.3	2.6	1.4
Experimental[a]		88.2 ± 0.5	99.0 ± 0.5	101.0 ± 0.5	88.1 ± 0.5			100.9 ± 0.5	100.5 ± 0.5	89.6 ± 0.5	110.6 ± 0.5	104.8 ± 0.5		

[a] Ref. [13]

Table 9 Enthalpies of reaction at 298 K in kcal/mol for the chain propagation reactions

Reaction		B3LYP	B3PW91	PBE0	M06	BMK	MP2	APNO	G4	CCSD(T)	Experimental
4	$C_3H_8 + H\cdot \rightarrow iC_3H_7\cdot + H_2$	−10.0	−8.1	−4.7	−4.2	−4.6	−0.4	−0.3	0.3	−6.4	−5.1
5	$C_3H_8 + H\cdot \rightarrow iC_3H_7\cdot + H_2$	−6.0	−4.1	−0.7	−0.7	−1.1	2.1	2.7	3.1	−3.1	−3.2
6	$C_3H_8 + CH_3\cdot \rightarrow iC_3H_7\cdot + CH_4$	−8.5	−8.6	−8.4	−8.7	−7.3	−5.0	−6.3	−6.6	−6.8	−5.7
7	$C_3H_8 + CH_3\cdot \rightarrow nC_3H_7\cdot + CH_4$	−4.5	−4.6	−4.4	−5.1	−3.8	−2.5	−3.3	−3.8	−3.6	−3.8
8	$iC_3H_7\cdot \rightarrow nC_3H_7\cdot$	−4.0	−4.0	−3.9	−3.6	−3.5	−2.5	−3.0	−2.8	−3.3	−1.9
12	$nC_3H_7\cdot \rightarrow C_2H_4 + CH_3\cdot$	20.4	24.2	27.5	26.7	24.9	24.5	24.0	23.2	23.4	23.5
19	$C_3H_8 + C_2H_3\cdot \rightarrow nC_3H_7\cdot + C_2H_4$	−9.6	−9.4	−9.3	−8.8	−8.9	−14.7	−9.0	−9.3	−11.0	−9.5
20	$C_3H_8 + C_2H_3\cdot \rightarrow iC_3H_7\cdot + C_2H_4$	−13.6	−13.4	−13.3	−12.4	−12.4	−17.1	−12.0	−12.1	−14.2	−11.4
21	$C_3H_8 + C_2H_3\cdot \rightarrow C_3H_6 + C_2H_5\cdot$	−12.1	−12.1	−11.9	−11.0	−12.4	−18.0	−12.8	−10.7	−13.8	−12.7
22	$C_3H_8 + C_2H_5\cdot \rightarrow nC_3H_7\cdot + C_2H_6$	0.2	0.2	0.3	0.3	0.4	0.5	0.3	0.0	0.3	0.5
23	$C_3H_8 + C_2H_5\cdot \rightarrow iC_3H_7\cdot + C_2H_6$	−3.8	−3.8	−3.7	−3.3	−3.1	−2.0	−2.7	−2.8	−2.9	−1.4
24	$C_3H_8 + C_3H_5\cdot \rightarrow nC_3H_7\cdot + C_3H_6$	16.1	15.7	15.7	15.2	14.5	8.1	13.9	14.9	12.3	12.9
25	$C_3H_8 + C_3H_5\cdot \rightarrow iC_3H_7\cdot + C_3H_6$	12.1	11.7	11.8	11.6	11.0	5.6	10.9	12.1	9.0	11.0
26	$C_3H_8 + nC_3H_7\cdot \rightarrow iC_3H_7\cdot + C_3H_8$	−4.0	−4.0	−3.9	−3.6	−3.5	−2.5	−3.0	−2.8	−3.3	−1.9
27	$nC_3H_7\cdot \rightarrow C_3H_6 + H\cdot$	35.2	36.2	36.7	36.6	33.6	29.2	32.6	34.5	33.3	33.1
28	$iC_3H_7\cdot \rightarrow C_3H_6 + H\cdot$	39.2	40.2	40.6	40.1	37.1	31.7	35.6	37.3	36.6	35.0
29	$C_3H_6 + H\cdot \rightarrow C_3H_5\cdot + H_2$	−22.1	−19.8	−17.4	−18.6	−15.6	−6.1	−16.5	−18.8	−15.4	−16.1
30	$C_3H_6 + H\cdot \rightarrow C_2H_3\cdot + CH_4$	−9.7	−7.1	−4.3	−6.6	−3.6	7.5	−2.9	−5.9	−2.5	−3.9
31	$C_3H_6 + CH_3\cdot \rightarrow C_3H_5\cdot + CH_4$	−20.6	−20.3	−20.2	−20.3	−18.2	−10.6	−17.2	−18.7	−15.9	−16.7
32	$C_3H_6 + CH_3\cdot \rightarrow C_2H_3\cdot + C_2H_6$	9.1	9.1	9.2	8.0	10.4	18.1	11.8	9.6	12.7	11.3
33	$C_3H_6 + C_2H_3\cdot \rightarrow C_3H_5 + C_2H_4$	−25.7	−25.1	−25.0	−24.1	−23.4	−22.8	−22.9	−24.2	−23.3	−22.4
34	$C_3H_6 + C_2H_5\cdot \rightarrow C_3H_5\cdot + C_2H_6$	−15.9	−15.5	−15.5	−14.9	−14.1	−7.7	−13.6	−14.9	−12.0	−12.4
35	$C_3H_6 + C_3H_5\cdot \rightarrow C_2H_3\cdot + C_4H_8$	28.3	27.9	27.7	26.2	28.2		26.5	25.8		25.2
36	$C_3H_6 + nC_3H_7\cdot \rightarrow C_2H_3\cdot + nC_4H_{10}$	11.9	11.9	11.7	10.6	12.1		12.4	10.5		12.2
37	$C_3H_6 + iC_3H_7\cdot \rightarrow C_2H_3\cdot + iC_4H_{10}$	15.0	15.0	14.4	12.3	14.2		13.4	11.3		12.1
38	$C_2H_6 + H\cdot \rightarrow C_2H_5\cdot + H_2$	−6.2	−4.3	−2.0	−3.7	−1.5	1.6	−2.9	−3.9	−3.4	−3.7
39	$C_2H_6 + CH_3\cdot \rightarrow C_2H_5\cdot + CH_4$	−4.8	−4.8	−4.7	−5.4	−4.1	−3.0	−3.6	−3.8	−3.9	−4.3
40	$C_2H_6 + C_2H_3\cdot \rightarrow C_2H_5\cdot + C_2H_4$	−9.8	−9.6	−9.6	−9.1	−9.3	−15.1	−9.3	−9.3	−11.3	−10.1
41	$C_2H_4 + H\cdot \rightarrow C_2H_5\cdot$	−37.7	−38.9	−39.2	−38.7	−37.1	−32.5	−36.4	−35.9	−36.2	−36.2
42	$C_2H_4 + CH_3\cdot \rightarrow C_2H_3\cdot + CH_4$	5.1	4.8	4.9	3.7	5.2	12.2	5.7	5.5	7.4	5.7
	MAD	6.0	5.2	5.6	5.2	2.9	11.3	1.4	2.7	2.8	
	RMSE	2.8	2.4	2.3	2.2	1.3	5.0	0.7	1.4	1.2	

The 6-311 ++G(3df,2pd) results are shown for DFT and ab initio calculations. Experimental data from Ref. [48]

$$4C_3H_8 \rightarrow 2CH_4 + C_2H_4 + nC_4H_{10} + iC_4H_{10}$$

which is not immediately obvious from the mechanism in Fig. 1. Experimentally, the enthalpy of this reaction is 14.7 kcal/mol, while the BMK method affords 17.8 kcal/mol. The three CBS methods result in 16.9, 14.9, and 15.9 kcal/mol, respectively, and the G4 result is 14.3 kcal/mol. The CBS-APNO and G4 results are closer to experiment for this non-elementary reaction.

In relation to the accepted mechanism, our main difference is the route by which the propyl radical is obtained. The calculations show that the direct H abstraction is an unfavorable process, because C–C bond scission requires less energy to proceed. However, once the methyl radicals are produced in this process, the reaction with propane is feasible, and both the n- and *i*-propyl radicals are formed. While this modification thus affords a mechanistic explanation, it does not modify greatly the whole dynamics of the process.

5 Conclusions

DFT, ab initio and model chemistry calculations have been performed on the chain initiation, propagation and termination reactions for the cracking of propane. From the methodological point of view, it was shown that the DFT BMK results of enthalpies of formation and energies of activation are very similar to the experimental values, with rms error of about 2 kcal/mol. For reactions involving

Table 10 Enthalpies of reaction at 298 K in kcal/mol for some of the termination reactions

Reaction		B3LYP	B3PW91	PBE0	M06	BMK	MP2	APNO	G4	CCSD(T)	Experimental
9a	$nC_3H_7\cdot + nC_3H_7\cdot \rightarrow nC_6H_{14}$	−78.4	−80.1	−83.0	−83.9	−86.8		−89.7	−87.5		−87.7
9b	$nC_3H_7\cdot + nC_3H_7\cdot \rightarrow C_3H_8 + C_3H_6$	−63.5	−61.5	−60.5	−62.2	−67.2	−70.8	−69.5	−66.2	−66.4	−67.9
10a	$iC_3H_7\cdot + iC_3H_7\cdot \rightarrow (CH_3)_2CHCH(CH_3)_2$	−69.2	−71.0	−74.8	−78.5	−81.3		−85.6	−84.0		−86.5
10b	$iC_3H_7\cdot + iC_3H_7\cdot \rightarrow C_3H_8 + C_3H_6$	−55.5	−53.4	−52.6	−55.0	−60.2	−65.9	−63.5	−60.5	−59.9	−64.1
11a	$iC_3H_7\cdot + nC_3H_7\cdot \rightarrow (CH_3)_2CH(CH_2)_2CH_3$	−74.3	−76.0	−79.4	−81.6	−83.8		−88.1	−86.1		−87.6
11b	$iC_3H_7\cdot + nC_3H_7\cdot \rightarrow C_3H_8 + C_3H_6$	−59.5	−57.5	−56.6	−58.6	−63.7	−68.3	−66.5	−63.4	−63.1	−66.0
43	$H\cdot + H\cdot \rightarrow H_2$	−104.7	−101.8	−98.9	−102.2	−101.9	−98.0	−104.7	−104.5	−102.8	−104.2
44	$CH_3\cdot + H\cdot \rightarrow CH_4$	−103.3	−102.2	−101.6	−103.8	−104.6	−102.5	−105.4	−104.5	−103.3	−104.8
45	$CH_3\cdot + CH_3\cdot \rightarrow C_2H_6$	−84.5	−86.0	−88.1	−89.2	−90.6	−91.9	−90.7	−89.0	−88.1	−89.6
46	$C_2H_3\cdot + H\cdot \rightarrow C_2H_4$	−108.3	−107.1	−106.5	−107.6	−109.7	−114.7	−111.1	−110.0	−110.7	−110.6
47	$C_2H_3\cdot + CH_3\cdot \rightarrow C_3H_6$	−93.5	−95.1	−97.3	−97.2	−101.0	−110.0	−102.5	−98.6	−100.8	−100.9
48	$C_2H_3\cdot + C_2H_3\cdot \rightarrow CH_2 = CHCH = CH_2$	−108.9	−110.3	−112.6	−111.4	−114.7		−116.2	−114.0		−116.0
49	$C_2H_5\cdot + H\cdot \rightarrow C_2H_6$	−98.5	−97.5	−96.9	−98.4	−100.5	−99.6	−101.8	−100.7	−99.4	−100.5
50	$C_2H_5\cdot + CH_3\cdot \rightarrow C_3H_8$	−81.5	−83.0	−85.4	−86.2	−88.6	−92.0	−89.7	−88.0	−87.0	−88.2
51	$C_2H_5\cdot + C_2H_3\cdot \rightarrow C_4H_8$	−92.1	−93.9	−96.3	−95.7	−98.8		−104.7	−98.6		−102.0
52	$C_2H_5\cdot + C_2H_5\cdot \rightarrow C_4H_{10}$	−78.4	−80.0	−82.7	−83.3	−86.5		−88.9	−87.1		−86.8
53	$CH_2CHCH_2\cdot + H\cdot \rightarrow CH_3CHCH_2$	−82.6	−82.0	−81.4	−83.5	−86.3	−91.9	−88.2	−85.8	−87.4	−88.1
54	$CH_3CHCH\cdot + H\cdot \rightarrow CH_3CHCH_2$	−108.2	−107.0	−106.5	−107.5	−110.9		−112.9	−109.5		
55	$CH_3CCH_2\cdot + H\cdot \rightarrow CH_3CHCH_2$	−103.0	−101.7	−101.2	−102.4	−106.2		−108.8	−105.4		
56	$CH_2CHCH_2\cdot + CH_3\cdot \rightarrow CH_3CH_2CH = CH_2$	−65.2	−67.2	−69.6	−71.0	−72.8		−76.0	−72.8		−75.9
57	$CH_3CHCH\cdot + CH_3\cdot \rightarrow CH_3CH = CHCH_3$	−92.7	−94.4	−96.6	−96.7	−98.9		−103.9	−97.8		
58	$CH_3CCH_2\cdot + CH_3\cdot \rightarrow (CH_3)_2C = CH_2$	−87.2	−88.8	−91.3	−92.0	−94.4		−101.2	−94.3		
56	$CH_2CHCH_2\cdot + C_2H_3\cdot \rightarrow CH_2 = CHCH_2CH = CH_2$	−94.1	−95.5	−151.8	−97.3	−101.1		−108.3	−101.6		
57	$CH_3CHCH\cdot + C_2H_3\cdot \rightarrow CH_3CH = CHCH = CH_2$	−83.3	−85.4	−87.8	−87.5	−90.1		−93.4	−90.1		−93.8
58	$CH_3CCH_2\cdot + C_2H_3\cdot \rightarrow CH_2 = CH\text{-}C(CH_3) = CH_2$	−100.8	−102.3	−105.1	−104.9	−108.0		−111.1	−108.7		
59	$CH_2CHCH_2\cdot + C_2H_5\cdot \rightarrow CH_3CH_2CH_2CH = CH_2$	−62.2	−64.2	−66.9	−68.1	−70.6		−75.2	−72.1		−74.3
60	$CH_3CHCH\cdot + C_2H_5\cdot \rightarrow CH_3CH = CHCH_2CH_3$	−89.3	−90.9	−93.5	−93.2	−95.6		−102.9	−96.6		
61	$CH_3CCH_2\cdot + C_2H_5\cdot \rightarrow CH_3CH_2C(CH_3) = CH_2$	−84.4	−85.8	−88.8	−89.5	−92.9		−96.8	−94.8		
	MAD	17.3	15.5	11.7	9.1	5.2	9.1	2.7	3.7	4.2	
	RMSE	8.3	7.6	6.3	5.0	2.4	4.2	1.2	2.0	1.9	

The 6-311 ++G(3df,2pd) results are shown for DFT and ab initio calculations. Experimental data from Ref. [48]

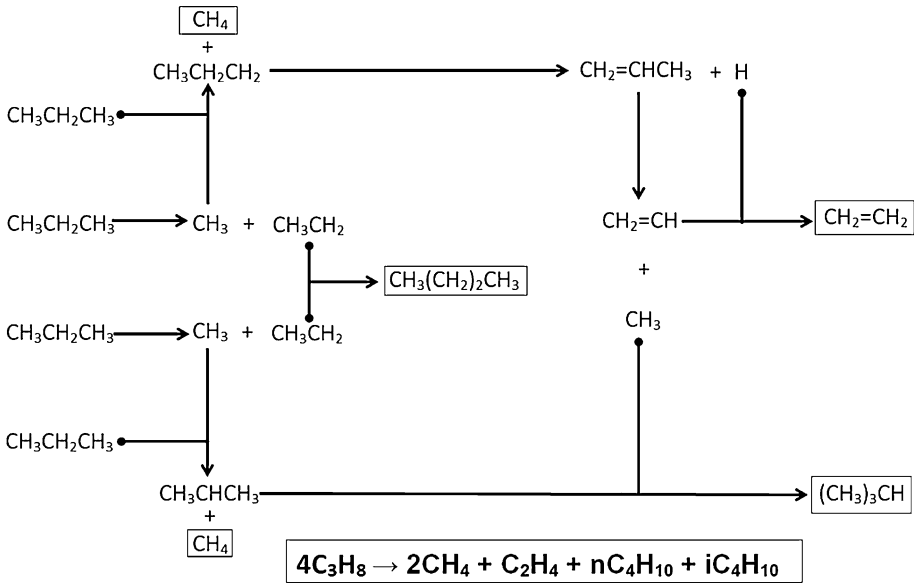

Fig. 7 Final scheme for the reduced mechanism (see *text*)

transition states, two- and three-parameter Arrhenius equations were calculated. It was shown that tunneling and internal rotation effects are important. Activation energies are then reproduced in good agreement with experimental ones. However, the preexponential factors calculated at the BMK level are too high, and the experimental relative concentration of radicals is then not reproduced accurately.

From the point of view of the reaction mechanism, calculations agree with the experimental result that the CC bond in propane is easier to break than the CH bonds. However, it was also shown that methyl radicals produced this way can abstract hydrogens from other propane molecules forming the *n*-propyl and *i*-propyl radicals. Although no attempt was performed in this paper to solve the full kinetic problem, a reduced mechanism is suggested, which proceeds through the formation of propene and ends up giving methane and butane, as observed experimentally.

Acknowledgments The authors acknowledge the financial support of CSIC, ANII, and Pedeciba through multiple grants.

References

1. Olah GA, Molnar A (2003) Hydrocarbon chemistry. Wiley, New York
2. Clymans PJ, Froment GF (1984) Comput Chem Eng 8:137
3. Hillewaert LP, Dierickx JL, Froment GF (1988) AIChE J 34:17
4. Ranzi E, Dente M, Plerucci S, Biardi G (1983) Ind Eng Chem Fund 22:132
5. Tsang W, Hampson RF (1986) J Phys Chem Ref Data 15:1087
6. Tsang W (1987) J Phys Chem Ref Data 16:471
7. Sabbe MK, Vandeputte AG, Reyniers M-F, van Speybroeck V, Waroquier M, Marin GB (2007) J Phys Chem A 111:8416
8. Zheng X, Blowers P (2006) Ind Eng Chem Res 45:530
9. Curran HJ (2006) Int J Chem Kinet 38:250
10. Hunter KC, East ALL (2002) J Phys Chem A 106:1346
11. Xiao Y, Longo JM, Hieshima GB, Hill RJ (1997) Ind Eng Chem Res 36:4033
12. Bencsura A, Knyazev VD, Xing S-B, Slagle IR, Gutman D (1992) Proc Combust Inst 24:629
13. Tsang W (1988) J Phys Chem Ref Data 17:887
14. Papic MM, Laidler KJ (1971) Can J Chem 49:535
15. Papic MM, Laidler KJ (1971) Can J Chem 49:549
16. Becke AD (1988) Phys Rev A 38:3098
17. Becke AD (1993) J Chem Phys 98:5648
18. Lee C, Yang W, Parr RG (1988) Phys Rev B 37:785
19. Perdew JP, Burke K, Wang Y (1996) Phys Rev B 54:16533
20. Perdew JP, Burke K, Ernzerhof M (1996) Phys Rev Lett 77:3865
21. Perdew JP, Burke K, Ernzerhof M (1997) Phys Rev Lett 78:1396
22. Adamo C, Barone V (1999) J Chem Phys 110:6158
23. Zhao Y, Truhlar DG (2008) Theor Chem Acc 120:215
24. Boese AD, Martin JML (2004) J Chem Phys 121:3405
25. Pople JA, Gill PMW, Johnson BG (1992) Chem Phys Lett 199:557
26. Johnson BG, Frisch MJ (1993) Chem Phys Lett 216:133
27. Johnson BG, Frisch MJ (1994) J Chem Phys 100:7429
28. Stratmann RE, Burant JC, Scuseria GE, Frisch MJ (1997) J Chem Phys 106:10175
29. Head-Gordon M, Pople JA, Frisch MJ (1988) Chem Phys Lett 153:503
30. Frisch MJ, Head-Gordon M, Pople JA (1990) Chem Phys Lett 166:275
31. Frisch MJ, Head-Gordon M, Pople JA (1990) Chem Phys Lett 166:281
32. Head-Gordon M, Head-Gordon T (1994) Chem Phys Lett 220:122
33. Bartlett RJ, Purvis GD III (1978) Int J Quantum Chem 14:561
34. Pople JA, Head-Gordon M, Raghavachari K (1987) J Chem Phys 87:5968
35. Nyden MR, Petersson GA (1981) J Chem Phys 75:1843
36. Petersson GA, Bennett A, Tensfeldt TG, Al-Laham MA, Shirley WA, Mantzaris J (1988) J Chem Phys 89:2193
37. Petersson GA, Al-Laham MA (1991) J Chem Phys 94:6081
38. Petersson GA, Tensfeldt TG, Montgomery JA Jr (1991) J Chem Phys 94:6091

39. Montgomery JA Jr, Frisch MJ, Ochterski JW, Petersson GA (2000) J Chem Phys 112:6532
40. Montgomery JA Jr, Frisch MJ, Ochterski JW, Petersson GA (1999) J Chem Phys 110:2822
41. Ochterski JW, Petersson GA, Montgomery JA Jr (1996) J Chem Phys 104:2598
42. Curtiss LA, Redfern PC, Raghavachari K (2007) J Chem Phys 126:084108
43. Eckart C (1930) Phys Rev 35:1303
44. Gaussian 09, Revision A.1, Frisch MJ, Trucks GW, Schlegel HB, Scuseria GE, Robb MA, Cheeseman JR, Scalmani G, Barone V, Mennucci B, Petersson GA, Nakatsuji H, Caricato M, Li X, Hratchian HP, Izmaylov AF, Bloino J, Zheng G, Sonnenberg JL, Hada M, Ehara M, Toyota K, Fukuda R, Hasegawa J, Ishida M, Nakajima T, Honda Y, Kitao O, Nakai H, Vreven T, Montgomery JA Jr, Peralta JE, Ogliaro F, Bearpark M, Heyd JJ, Brothers E, Kudin KN, Staroverov VN, Kobayashi R, Normand J, Raghavachari K, Rendell A, Burant JC, Iyengar SS, Tomasi J, Cossi M, Rega, Millam NJ, Klene M, Knox JE, Cross JB, Bakken V, Adamo C, Jaramillo J, Gomperts RE, Stratmann O, Yazyev AJ, Austin R, Cammi C, Pomelli JW, Ochterski R, Martin RL, Morokuma K, Zakrzewski VG, Voth GA, Salvador P, Dannenberg JJ, Dapprich S, Daniels AD, Farkas O, Foresman JB, Ortiz JV, Cioslowski J, Fox DJ (2009) Gaussian, Inc., Wallingford
45. Ghysels A, Verstraelen T, Hemelsoet K, Waroquier M, Van Speybroeck V (2010) J Chem Inf Model 50:1736
46. Sundaram KM, Froment GF (1979) Chem Eng Sci 34:635
47. Van Damme PS, Narayanan S, Froment GF (1975) AIChE J 21:1065
48. Linstrom PJ, Mallard WG, Eds (2003) NIST Chemistry WebBook, NIST Standard Reference Database Number 69, National Institute of Standards and Technology, Gaithersburg MD, 20899, http://webbook.nist.gov
49. Zheng X (2006) A computational investigation of hydrocarbon cracking: gas phase and heterogeneous catalytic reactions on zeolites, PhD Dissertation, University of Arizona, Tucson, Arizona
50. Zheng X, Blowers P (2005) Mol Simul 31:979
51. Baldwin RR, Walker RW (1979) J Chem Soc Faraday Trans 75:140
52. Kerr JA, Parsonage MJ (1976) Evaluated kinetic data on gas phase hydrogen transfer reactions of methyl radicals. Butterworths, London
53. Matheu DM, Green WH, Grenda JM (2003) Int J Chem Kinet 35:95
54. Berkley RE, Woodall GNC, Strausz OP (1969) Gunning HE 47:3305
55. Tsang W (1985) J Am Chem Soc 107:2872
56. Dean AM (1985) J Phys Chem 89:4600
57. Mintz KJ, Le Roy DJ (1978) Can J Chem 56:941
58. Camilleri P, Marshall RM, Purnell H (1975) J Chem Soc Faraday Trans I(71):1491
59. Lin MC, Laidler KJ (1966) Can J Chem 44:2927
60. Kerr JA, Calvery JG (1961) J Am Chem Soc 83:3391
61. Saeys M, Reyniers MF, Marin GB, Van Speybroeck V, Waroquier M (2004) AIChE J 50:426
62. Hogg AM, Kebarle P (1964) J Am Chem Soc 86:4558
63. Baulch DL, Cobos CJ, Cox RA, Esser C, Frank P, Just Th, Kerr JA, Pilling MJ, Troe J, Walker RW, Warnatz J (1992) J Phys Chem Ref Data 21:411
64. Leathard DA, Purnell JH (1968) Proc R Soc Lond A 306:553